Numerical Simulation of Microwave-Sustained Supersonic Plasmas for Application to Space Propulsion*

V.P. Chiravalle†, **R.B. Miles**‡, and **E.Y. Choueiri**§
Princeton University, Princeton, New Jersey 08544

AIAA-2001-0962¶

Abstract

The concept of adding energy to an expanding supersonic flow using a microwave-sustained plasma is explored numerically by solving the complete system of both the Maxwell equations and the Navier Stokes equations for the case of an argon flow in a realistic thruster geometry. Results show that when an additional amount of power, equal to 45 % of the power deposited in the plenum, is added to the supersonic flow a toroidal plasma forms, but only a 3 % increase in specific impulse is achieved. It is concluded that future work relating to this concept should concentrate on finding ways to confine the plasma to the centerline.

*This research was funded by an AASERT grant from AFOSR with additional support from NSF.

†Graduate Student, Mechanical & Aerospace Engineering, AIAA

‡Professor, Mechanical & Aerospace Engineering, Associate Fellow AIAA

§Assistant Professor, Mechanical & Aerospace Engineering, Senior Member AIAA

¶Presented at the 39^{th} AIAA Aerospace Sciences Meeting and Exhibit, Reno, NV, January 8-11, 2001. Copyright by authors. Published by the AIAA with permission.

1 Introduction

1.1 Motivation

The conventional approach for electrothermal space propulsion systems has been to heat a propellant gas to a high temperature in the plenum and then to expand the flow in a nozzle and produce thrust. Examples of such systems are resistojets, arcjets, and microwave electrothermal thrusters. For all these systems, the specific impulse is limited to the maximum average temperature that can be achieved by heating a low molecular weight propellant in the plenum. For a state of the art 2 kW hydrazine arcjet the specific impulse is roughly 600 sec[1]. Both arcjets and microwave electrothermal thrusters make use of a high temperature plasma to heat the flow. The plasma in an arcjet is sustained by electric current emitted from a cathode; in the case of a microwave electrothermal thruster, microwave energy is used to sustain the plasma. The fact that a microwave-sustained plasma can be created without electrodes and can be maintained away from the material surfaces of the thruster, may allow for large reductions in thruster erosion and significant improvements in overall lifetime, compared with arcjets. From a fundamental point of view the maximum average temperature that can be achieved for a given propellant in a microwave

electrothermal thruster is limited by the reflection of microwave power from the plasma, an effect that gets more pronounced as the temperature and electron density of the gas increases. One possible way to circumvent this limitation and to realize higher performance in terms of specific impulse and thrust is to add additional energy to the propellant in the supersonic region of the flow, creating a supersonic "afterburner". This can be accomplished by using additional microwave energy to create another plasma in the supersonic region of flow. To date numerical simulation of microwave-sustained plasmas has concentrated on the high pressure, subsonic regime[2]. The goal of the present work is to apply a computational model of similar sophistication as existing models in the supersonic regime and to show a case where a stable microwave-sustained argon plasma at 2.45 GHz can exist under these conditions as well.

1.2 Previous Work

Unlike resistojets and arcjets, which have been studied extensively for more than thirty years and have matured to the point of routine utilization in various spaceflight operations, microwave electrothermal thrusters have yet to be tested in space. The physics of microwave-sustained discharges at high pressures in subsonic flows has been a topic of research for many years and is well understood[3]. Different configurations have been explored for coupling microwave power to a gas, the most promising for thruster applications is the cylindrical resonant cavity design, employing either the TM_{011} or TM_{012} microwave mode structure. The first thruster of this kind was build in the early 1980's and it consisted of a cylindrical microwave resonant cavity at 2.45 GHz and a quartz tube, arranged concentrically[4]. He or N_2 gas flowed through the quartz tube, where the walls stabilized the microwave plasma on the centerline. The gas then exited through a quartz nozzle connected to the tube. It was shown that the ratio of power absorbed by the plasma to the incident power delivered to the cavity, the microwave coupling efficiency, could be made to exceed 95% with proper tuning of the cavity for discharges sustained at pressures from 40 to 1000 torr. Excessive heating and erosion of the quartz nozzle limited the input power to less than 2 kW for mass flow rates in the range of 100 mg/sec. Another prototype thruster utilizing a cylindrical resonant cavity at 2.45 Ghz with a free-floating plasma inside the cavity has operated successfully at power levels of up to 2.2 kW and pressures as high as 3 atm with He, N_2, NH_3 and H_2 as propellants[5]. In that design the plasma is stabilized by flow swirl created from tangential gas injection into the cavity. The gas exits the cavity through a graphite nozzle. Spectroscopic measurements were made of free-floating He plasmas in the cavity, stabilized by a bluff body, and the results indicate that the electron temperature of these discharges is roughly constant at 12,000 K over a range of incident powers from 0.5 to 1.0 kW and a range of pressures from 1.0 to 3.0 atm[6].

In addition to these experimental efforts, numerical work has been done to model the physical processes occurring in microwave-sustained discharges. The size, shape, location and peak temperature of the free-floating He discharges, stabilized by a bluff body, discussed above have been reasonably well predicted by a computational model consisting of a low Mach number formulation of the Navier Stokes and the Maxwell equations[2]. In a TM_{011} or TM_{012} resonant cavity the oscillating electric field has both a radial and an axial component, and the magnetic field has an azimuthal component. In that work the parabolized Navier Stokes equations were solved by a time-implicit finite difference technique, and the Maxwell equations relating the three electromagnetic field components were solved using a time-explicit finite difference technique. The time dependent solu-

tion for the electromagnetic field was then averaged over several wave periods to obtain energy addition terms for the fluid equations. Thermodynamic equilibrium was assumed, in the sense that both electrons and heavy species have the same temperature and that the electron concentration is determined from the Saha relation. Subsequently, the model was extended to include a converging flow geometry so that realistic thruster configurations could be simulated, and a parametric study of the effect of nozzle throat area, discharge pressure and absorbed power on the location of the plasma in a resonant cavity thruster was performed[7]. For simulations at a microwave frequency of 0.915 GHz, a helium mass flow rate of 1.9 g/sec (1 atm plenum pressure) and an incident power of 40 KW, a toroidal plasma was observed off the cavity centerline. As the cavity length was changed, detuning the cavity from resonance and reducing the power absorbed by the plasma, it was shown that the plasma would move back on the centerline.

1.3 Outline

The physical model and the numerical techniques used in the present study are described briefly in §2. The results from a computation of a microwave sustained supersonic argon plasma, are presented in §3. The validity of a critical model assumption, that electrons and heavy species have the same temperature, is discussed in §4.

2 Physical Model

The physical model used in this work shares many common features with the model of Ref. [2], there are some important differences, however. In both cases a fluid model is coupled to a electromagnetic model that solves the Maxwell equations. In the previous work high pressure, low Mach number flows were considered, where the solution of the parabolized Navier Stokes equations could be considered adequate. In this work the complete set of Navier Stokes equations are solved, using modern CFD techniques. In the work of Ref. [2] the Maxwell equations are solved using a time marching technique, in contrast to the finite element approach pursued in this work. In addition because the electromagnetic field relations are formulated in terms of the Helmholtz wave equation in this work, it is necessary only to solve for the two components of the electric field. One point of similarity is that both models assume thermodynamic equilibrium, and all transport properties and the plasma conductivity are calculated accordingly in both cases. This may be a point were both models fail, however, since at least for the problem considered here it is shown in §4, that in the region of intense energy addition the results are not consistent with equilibrium conditions.

2.1 Flowfield Configuration

Argon was chosen as the propellant gas of interest in this study purely to illustrate the supersonic energy addition concept; a practical electrothermal thruster would use a low molecular weight gas. The geometry of the problem considered here is illustrated in Fig. 1. Argon, at a flow rate of 200 mg/sec, enters a conical nozzle with a half angle of $15\,\mathrm{deg}$, an inlet radius of 0.0625 in, and a length of 0.8 in. These dimensions represent a realistic nozzle geometry. Sonic conditions are assumed at the gas injection port where the temperature is 5000 K and the pressure is 0.2 atm. These conditions correspond to the addition of 670 W of power in the subsonic plenum section of this hypothetical thruster. The nozzle is concentric with a cylindrical waveguide with a radius of 3.0 in. In Fig. 1 a plasma is shown inside the nozzle region, labeled Section A. The Navier Stokes equations are

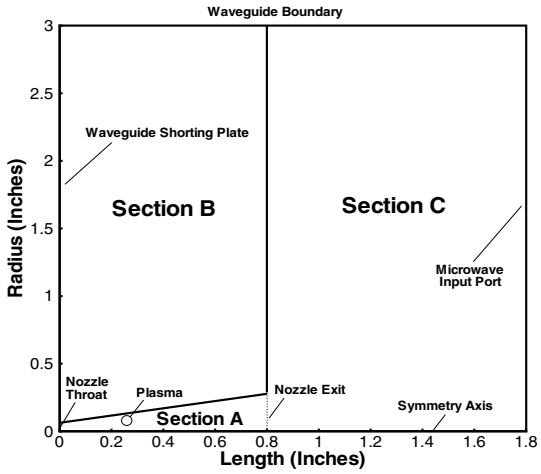

Figure 1: Diagram showing the geometry of the numerical simulation.

solved in section A. The microwave field is computed throughout the entire waveguide, sections A, B and C. It is assumed that the walls of the waveguide and the shorting plate, which lies along the y-axis in Fig. 1, are perfect conductors. The walls of the nozzle are labeled Section B in Fig. 1 and consist of alumina ceramic, which has a dielectric constant of 9.0. The nozzle walls fill the entire cross section of the waveguide. A real microwave thruster would have a radial antenna protruding into section B, which would act to couple microwave energy into the cavity. The three dimensional field pattern associated with a radial antenna is not considered in the present model, but rather a microwave transmission region, labeled Section C, is added to the computational domain so that microwave energy can propagate from the microwave input port into the regions of interest, sections A and B. There is no interaction between the exhaust gas and the microwave field in section C. It is assumed that gas which has moved through the nozzle exhausts into a perfect vacuum. The value of the complex electric field is specified at the microwave input port, using the theoretical expression for a cylindrical TM_{01} mode with the amplitude chosen so that a desired value of total power is absorbed by the plasma. The present case assumes that an additional 300 W of power is absorbed by the plasma in the supersonic section. Now the equations that describe the fluid variables and the microwave field components are discussed along with the numerical techniques used to solve them.

2.2 Navier Stokes Equations

The unsteady axisymmetric Navier Stokes equations, which describe the conservation laws of mass, momentum and energy for the gas in the nozzle, can be written in cylindrical coordinates in the follow differential vector form[8]

$$\frac{\partial r\mathbf{U}}{\partial t} + \frac{\partial r\mathbf{F}(\mathbf{U})}{\partial x} + \frac{\partial r\mathbf{G}(\mathbf{U})}{\partial r} = \mathbf{S}, \qquad (1)$$

where x and r are the axial and radial directions, respectively. $\mathbf{U} = (\rho, u, v, E)^{\mathrm{T}}$ is the vector of conservation variables, with gas density as ρ, axial velocity as u, radial velocity as v and total energy density (thermal plus kinetic) as E. The flux vectors, $\mathbf{F}(\mathbf{U}) = \mathbf{F^c}(\mathbf{U}) + \mathbf{F^d}(\mathbf{U})$ and $\mathbf{G}(\mathbf{U}) = \mathbf{G^c}(\mathbf{U}) + \mathbf{G^d}(\mathbf{U})$, are functions of the conservation variables and contain both convective and diffusive terms. The convective flux vectors are

$$\mathbf{F^c}(\mathbf{U}) = \begin{bmatrix} \rho u \\ \rho u^2 + p \\ \rho uv \\ u(E+p) \end{bmatrix},$$

$$\mathbf{G^c}(\mathbf{U}) = \begin{bmatrix} \rho v \\ \rho uv \\ \rho v^2 + p \\ v(E+p) \end{bmatrix},$$

while the diffusive flux vectors are

$$\mathbf{F^d}(\mathbf{U}) = \begin{bmatrix} 0 \\ \tau_{xx} \\ \tau_{xr} \\ -q_x + u\tau_{xx} + v\tau_{xr} \end{bmatrix},$$

$$\mathbf{G^d}(\mathbf{U}) = \begin{bmatrix} 0 \\ \tau_{xr} \\ \tau_{rr} \\ -q_r + u\tau_{xr} + v\tau_{rr} \end{bmatrix}.$$

In the previous relations p is the gas pressure. The viscous stresses are given by

$$\begin{aligned} \tau_{xx} &= \frac{4}{3}\mu\frac{\partial u}{\partial x} - \frac{2}{3}\mu\left(\frac{\partial v}{\partial r} + \frac{v}{r}\right), \\ \tau_{rr} &= \frac{4}{3}\mu\frac{\partial v}{\partial r} - \frac{2}{3}\mu\left(\frac{\partial u}{\partial x} + \frac{v}{r}\right), \\ \tau_{xr} &= \mu\left(\frac{\partial u}{\partial r} + \frac{\partial v}{\partial x}\right), \end{aligned}$$

with μ equal to the viscosity. The heat fluxes are

$$\begin{aligned} q_x &= -k\frac{\partial T}{\partial x}, \\ q_y &= -k\frac{\partial T}{\partial r}, \end{aligned}$$

with T equal to the gas temperature and k equal to the thermal conductivity. The right hand side of the equation, $\mathbf{S}$, contains source terms that are due to cylindrical symmetry of the problem and the microwave energy addition term; its functional form is given below

$$\mathbf{S} = \begin{bmatrix} 0 \\ 0 \\ p + \frac{2}{3}\left(\tau_{xr} - \frac{2\mu v}{r}\right) \\ \langle \mathbf{i} \cdot \mathbf{E} \rangle \end{bmatrix}.$$

In the above expression $\mathbf{i}$ is the current density vector and $\mathbf{E}$ is the electric field vector. The microwave energy addition term $\langle \mathbf{i} \cdot \mathbf{E} \rangle$ is described in §2.3.

A conservative finite volume numerical discretization is used to integrate the governing equations(1) in time until a steady state is reached, an approach that has been thoroughly validated by several authors[8, 9, 10]. The conservative variables $\mathbf{U}$ are stored at the center of each cell on the grid and updated after each time step. The convective and diffusive fluxes are evaluated separately at the boundaries of each cell. A flux limited scalar dissipation technique has been employed to ensure that non-linear stability criteria are satisfied[9]. A simple Euler finite difference is used for marching forward in time, with the largest time step size determined as discussed in Ref. [9]. The Navier Stokes code performs bilinear interpolation from values stored in a table, to compute the equation of state and the transport properties in the equations above. These properties are stored as functions of gas density and internal energy (energy per unit mass). The interpolation table for argon, used for the calculations in this paper, was generated by a widely used and well validated chemical equilibrium code, described in Ref. [11].

2.3 Maxwell Equations

As mentioned previously, for a TM_{01} mode in a cylindrical waveguide there are three components of the electromagnetic field, E_r, E_z, and H_θ. The relationships among these components are expressed by the Maxwell equations. When considering a time periodic electromagnetic field of angular frequency ω it is convenient to describe any one of the components of the field, represented by Φ, in terms of a complex amplitude, in the following way

$$\Phi = \frac{1}{2}\left(\phi e^{-i\omega t} + \phi^* e^{i\omega t}\right). \tag{2}$$

By writing each component in the form of Eqn. 2, substituting into the Maxwell equations and simplifying it can be shown that the complex amplitude of

each of the three components of the electromagentic field obeys the Helmholtz wave equation. For a problem involving microwave energy addition to a plasma, only the electric field components need to be determined, as will be discussed shortly. In cylindrical coordinates the Helmholtz equation for the complex amplitude of the axial electric field, E_z is

$$\frac{1}{r}\frac{\partial}{\partial r}r\frac{\partial E_z}{\partial r}+\frac{\partial^2 E_z}{\partial x^2}+\beta^2 E_z=0. \tag{3}$$

The corresponding equation for the complex amplitude of the radial component, E_r is

$$\frac{1}{r}\frac{\partial}{\partial r}r\frac{\partial E_r}{\partial r}+\frac{\partial^2 E_r}{\partial x^2}+\left(\beta^2-\frac{1}{r^2}\right)E_r=0. \tag{4}$$

In these equations the complex propagation constant β is such that $\beta^2 = \frac{\omega^2}{c^2}\left(1-i\frac{\sigma}{\epsilon_0\omega}\right)$, where c is the speed of light, ϵ_0 is the dielectric permitivity of free space and σ is the complex conductivity of the plasma.

The complex conductivity is responsible for the coupling between fluid and the microwave field. The complex conductivity is a function of the electron number density N_e and total electron collision frequency ν according to the following expression

$$\sigma=\frac{N_e e^2}{m_e\left(\nu+i\omega\right)}, \tag{5}$$

where e is the electron charge and m_e is the mass of an electron. Assuming equilibrium conditions the total collision frequency is a function of the gas temperature T, the electron number density N_e and the atomic number density N_A, as discussed in Ref. [12]

$$\nu=6.2\times10^3\sigma_{eh}\sqrt{T}N_A+3.0\times10^{-5}N_e T^{-3/2}. \tag{6}$$

The first term in the equation above represents the contribution from electron-atom collisions and the second term represents the contribution from electron-ion collisions. In this work the electron-atom collision cross section σ_{eh} was taken to be $10^{-20}\mathrm{m}^2$. Having determined σ using the above formula, the volume energy addition term is determined as given below

$$\langle \mathbf{i}\cdot\mathbf{E}\rangle=\frac{1}{4}\left(\sigma+\sigma^*\right)\left(E_r E_r^*+E_z E_z^*\right). \tag{7}$$

The finite element method is used to solve both Eqn. (4) and Eqn. (3) separately. This method breaks the two dimensional computational domain (x,r plane) into finite elements and assumes, at any point inside one of these finite elements, that an electric field component can be expressed as a weighted average of its respective value at the corners of that particular finite element. Quadrilateral finite elements are used in this work, and first order bilinear interpolation functions are used as the basis functions for the weighted averaging. In solving both for E_r and E_z a matrix is generated, implicitly relating the values of E_r and E_z respectively at every point on the grid. These matrices are inverted using a standard numerical algorithm for band-diagonal matrices.

2.4 Boundary Conditions

In this section the boundary conditions for the quantities in the calculation are reviewed, starting first with the microwave fields. The finite element method requires that at a boundary either the function itself or its derivative is specified. At the inlet port the values of E_r and E_z are specified, as discussed in the previous section. Along the waveguide boundary it is assumed that $E_z = 0$, since tangential electric fields cannot exist on the surface of a perfect conductor. The corresponding boundary condition for the radial electric field is $\partial r E_r/\partial r = 0$. Along the shorting plate boundary the following conditions hold true, $E_r = 0$ and $\partial E_z/\partial z = 0$. Finally at the waveguide centerline, the cylindrical symmetry of the problem implies that $E_r = 0$ and $\partial E_z/\partial r = 0$.

Now the boundary conditions for the fluid variables are discussed. Because of the cell-centered scheme used by the Navier Stokes solver it is necessary to specify the values of the convective fluxes, $\mathbf{F^c}(\mathbf{U})$ and $\mathbf{G^c}(\mathbf{U})$, at the physical boundaries of the nozzle domain. At the nozzle throat the values of the convective fluxes are specified, corresponding to sonic flow at 5000 K and 0.2 atm. At the nozzle exit the convective fluxes are calculated based on the values of the conservative variables $\mathbf{U}$, at the adjacent cell centers. Along the nozzle wall and centerline boundaries the convective fluxes are specified so that there is no mass, momentum or energy flux through these respective boundaries. In addition to the above specifications for the convective fluxes, the no slip conditions, $u = 0$ and $v = 0$, are applied at the nozzle wall boundary and the temperature of the nozzle wall is fixed at 500 K. This facilitates the computation of the diffusive fluxes, $\mathbf{F^d}(\mathbf{U})$ and $\mathbf{G^d}(\mathbf{U})$, at these locations. It is assumed that the diffusive fluxes are zero at the gas inlet and exit ports. At the nozzle centerline the diffusive fluxes are calculated by extrapolating the values of $\partial u/\partial x$ and $\partial T/\partial x$ from the interior domain, and enforcing cylindrical symmetry, by setting v and all partial derivatives with respect to r equal to zero.

3 Simulation Results

The numerical problem formulated in the previous section was solved using a desktop computer, and the results are now presented.

The time-averaged values of the axial electric field, $\frac{1}{2}\left(E_z E_z^*\right)$ are presented in Fig. 2 for the case when a plasma is present in the nozzle. There are two areas of maximum field intensity in Fig. 2, one that is entirely inside the alumina nozzle region, section B in Fig. 1, and one that spans both sections B and C. The plasma forms in the region between these two maxima. The maximum field strength is roughly 0.55 kV/cm. The corresponding time-averaged value of the radial field is shown in Fig. 3. In the case without a plasma, there is no change in the radial field. The axial field, however, shows a distinct difference as illustrated in Fig. 4. The maxima inside the nozzle has a straight boundary at about $x = 0.4$ in when the plasma is not present. When the plasma forms it deforms this boundary, pushing the electric field contours to the left, away from the interior of the plasma. This effect is exactly what would be expected if a metal conductor were placed inside the nozzle at this location. In choosing the geometry of the problem in this paper, it was the intention to model the electric fields in a resonant cavity thruster as closely as possible. This goal has been achieved because the radial field in Fig. 3 drops off to zero at the interface between the alumina nozzle and the microwave transmission section, $x = 0.8$ in, and if another shorting plate were placed in the waveguide at this location a resonant cavity would be created.

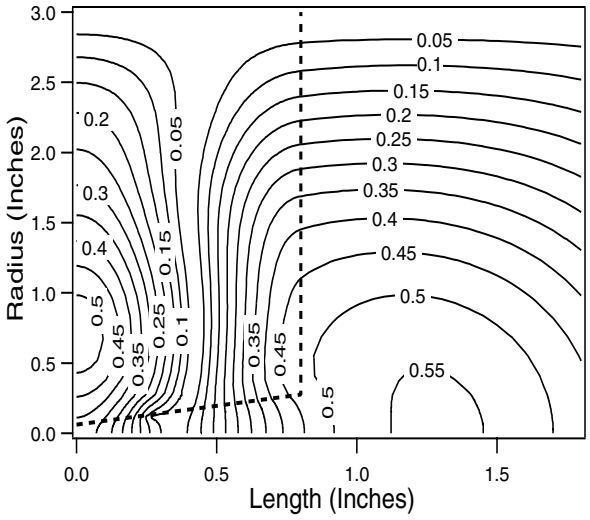

Figure 2: Time-averaged value of the axial electric field with a plasma inside the nozzle.

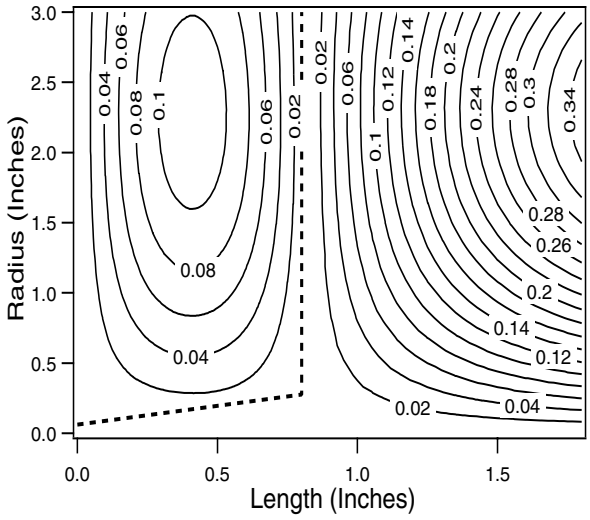

Figure 3: Time-averaged value of the radial electric field.

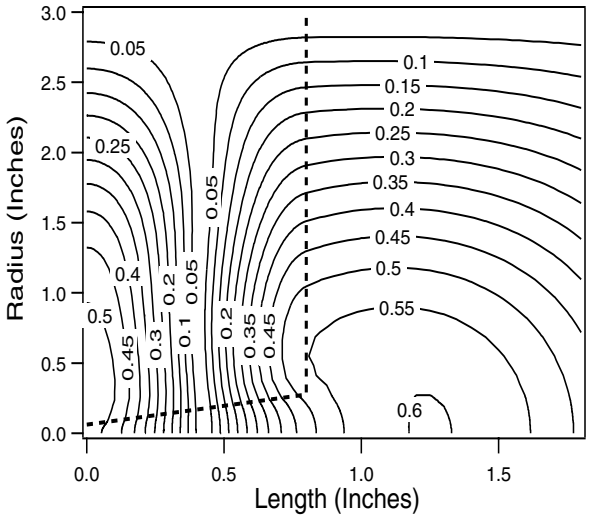

Figure 4: Time-averaged value of the axial electric field without a plasma inside the nozzle.

The physical properties of the plasma are now discussed. The plasma has a toroidal shape located relatively close to the nozzle wall as evidenced by the temperature contours presented in Fig. 5. In this regard the plasma seen here is similar to some of the plasmas computed in Ref. [7]. The maximum temperature is about 9100 K, at a location of $x = 0.27$ in and $y = 0.12$ in. This temperature is more than 4000 K hotter than the temperature at the gas inlet. The corresponding pressure at this location is about 26 torr. The pressure contours are shown in Fig. 6. A shock structure is established in the nozzle due to the energy addition, as evidenced by the pressure rise along the nozzle centerline at about $x = 0.4$ in. The pressure at the exit of the nozzle is roughly 1 torr and the Mach number close to the centerline at the exit is about 5, as shown in Fig. 7. The hottest point of the plasma, the 9100 K point, occurs where the Mach number is 0.52. The electron number density at this point is about 10^{15} cm^{-3}, as indicated in Fig. 8. This electron number density corresponds to an ionization fraction of about 4.1%. Moving 0.1 inches downstream of this point the electron number density drops by four orders of magnitude to roughly 10^{11} cm^{-3}. The volume heating rate at the maximum temperature point is 43 $\mathrm{kW/cm}^3$. A maximum volume heating rate of 68 $\mathrm{kW/cm}^{-3}$ occurs at a point slightly upstream of the maximum temperature point. The Mach number at this point is 0.29. Most of the energy addition occurs in the subsonic viscous boundary layer.

Without a plasma the thrust of this hypothetical thruster is 0.451 N and with a 300 W plasma in the supersonic section, the thrust is 0.464 N. The corresponding values of specific impulse with and without energy addition are 227 sec and 233 sec respectively. The total power (300 W) added to the supersonic flow as a percentage of the 670 W input power in the plenum is 45%, which results in only a 3 % increase in thrust and specific impulse. 79 % of the power added to the plasma in the supersonic section, 237 W, is removed by conduction through the

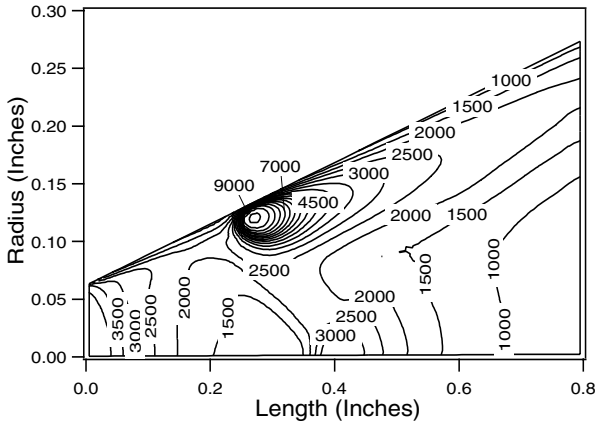

Figure 5: Temperature contours in K for the flow inside the nozzle.

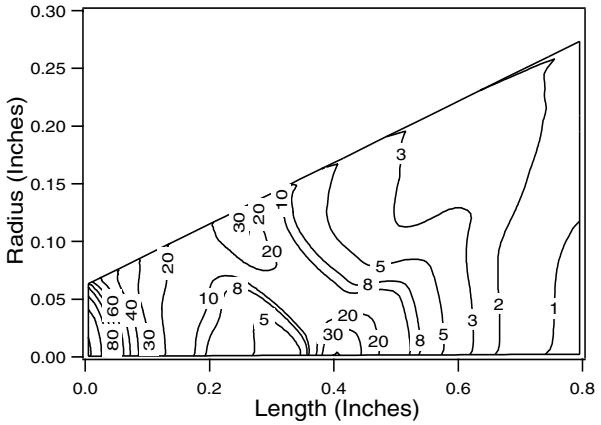

Figure 6: Pressure contours in torr for the flow inside the nozzle.

nozzle wall, assuming that the nozzle wall is maintained at 500 K. A real ceramic nozzle in this situation would have a two dimensional temperature profile and the maximum temperature would probably be higher than what was assumed in these calculations. A higher wall temperature would make the supersonic energy addition process more efficient. It is, of course, more desirable if the plasma were kept away from the nozzle wall altogether, confined in some way to the centerline of the flow.

4 Investigation of Model Assumptions

The validity of some of the assumptions in the model are now explored. For the Navier Stokes equations or for any fluid approximation to be valid, the characteristic length and time scales must be larger than the length and time scales associated with collisions on an atomic level. In this work the characteristic length L_c is defined in terms of the gas temperature T as $\frac{T}{\partial T/\partial x}$ and the characteristic time is defined as $t_c = L_c/u$. The mean free path of argon atoms can be estimated with the formula $\lambda_p = 1/N_A\sqrt{2}\pi d^2$, where d is the diameter of an argon atom. In this work d is taken to 4×10^{-10} m. The ratio L_c/λ_p throughout the entire flow field is never less than 10, and in most of the domain it is greater than 100. A typical value for the characteristic length in the region just before the gas exhaust port is about 0.8 in and in the plasma it is roughly 0.2 in. This indicates that fluid theory is accurate, at least in describing the heavy particle species. Using the values of total electron collision frequency it is possible to find $t_c\nu$. $t_c\nu$ is everywhere greater than 100, and in the region where the plasma is located it is closer to 10^6. From this it is obvious that a fluid description of the electrons is accurate as well.

One final question is whether both the electrons and the heavy particles do indeed have the same temperature, as assumed in this work. This can be accomplished by considering what the electron temperature would need to be in order for all the energy absorbed by the electrons from the microwave field, equal to $\langle \mathbf{i} \cdot \mathbf{E} \rangle$, to be transferred to the heavy particles through elastic collisions. The rate of energy

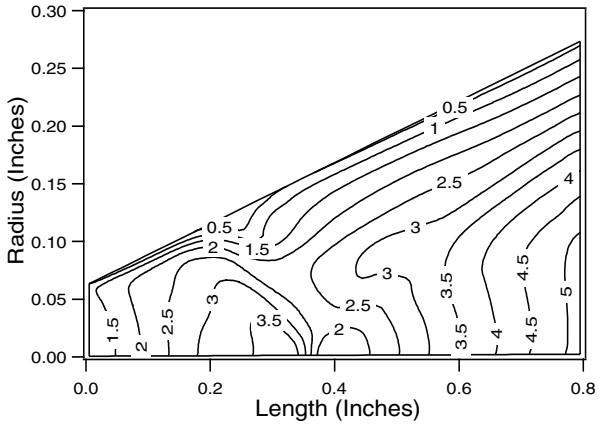

Figure 7: Mach number contours for the flow inside the nozzle.

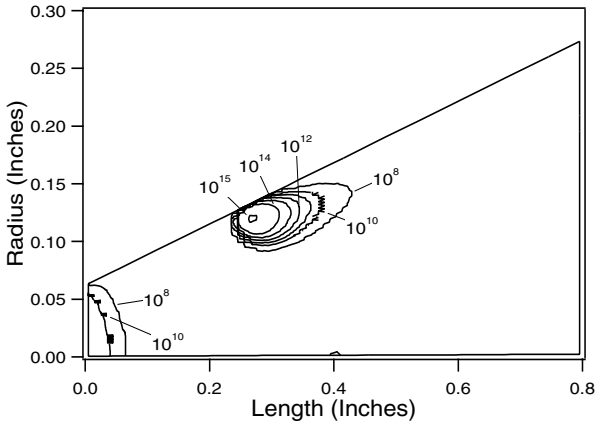

Figure 8: Electron number density contours in cm^{-3} for the flow inside the nozzle.

transfer is determined by the following formula

$$\xi = 3k_b N_e \nu \frac{m_e}{m_A} \left(T_e - T\right), \tag{8}$$

where k_b is the Boltzman constant, m_A is the mass of an argon atom (or ion) and T_e is the electron temperature. Taking the values of heavy species temperature T, volume heating rate and gas density computed by the numerical model it is possible to solve Eqn. (8) for the electron temperature, if it is further assumed that the ionization level is determined by the gas density and the electron temperature (instead of the heavy species temperature) according the Saha equilibrium relation. When this is done for a point close to the maximum temperature point of the plasma, the electron temperature is found to be roughly $1.5\mathrm{eV}$ (17,000 K), which is significantly higher than the heavy species temperature (9100 K). The corresponding electron number density is $4 \times 10^{16}\mathrm{cm}^{-3}$, which is about an order of magnitude higher than the value predicted assuming that the electrons and heavy species have the same temperature. Therefore, at the density levels associated with this expanding flow in order for all the energy absorbed by the electrons to be transferred to the heavy particles it is necessary for a certain degree of non-equilibrium to exist.

5 Conclusions

A fully coupled calculation, solving both the Navier Stokes and Maxwell equations has been performed for a supersonic argon flow in a realistic thruster geometry, expanding upon research done on subsonic plasmas. Like certain situations involving subsonic microwave-sustained plasmas, the plasma in this calculation has a toroidal shape and is located relatively close to the nozzle wall in the viscous boundary layer. The maximum temperature in this plasma is about 9100 K and the electron number density is roughly $10^{15}\mathrm{cm}^{-3}$. The presence of such a plasma distorts the axial electric field pattern in the thruster, forcing the electric field out of the region where the plasma is located. It has been shown that most of the energy added to this supersonic plasma is conducted through the nozzle walls, in this case where the wall temperature is 500 K. The specific impulse of this hypothet-

ical thruster increased, nevertheless, from 227 sec to 233 sec. Future work with this problem should concentrate on finding a way to confine the plasma to the nozzle centerline, if it is possible to do so. Finally a check was performed to verify the validity of the continuum fluid assumption and the approximation that the electron and heavy species temperatures are the same. There is conclusive evidence that the continuum fluid assumption is valid for both electrons and heavy particles, whereas the assumption of a single fluid temperature is inaccurate. Therefore it is recommended that a model including separate temperatures for both the heavy species and the electrons be applied to this problem.

References

[1] P. G. Lichon and J. M. Sankovic. Development and demonstartion of a 600-sec mission-average i_{sp} arcjet. *Journal of Propulsion and Power*, 12:1018–1025, 1996.

[2] S. Venkateswaran and C. L. Merkle. Numerical investigation of bluff-body stabilized microwave plasams. *Journal of Propulsion and Power*, 11:357–364, 1995.

[3] Y. P. Raizer. *Gas Discharge Physics*. Springer-Verlag, 1997.

[4] S. Whitehair and J. Asmussen. Microwave electrothermal thruster performance in helium gas. *Journal of Propulsion and Power*, 3:136–144, 1985.

[5] D. J. Sullivan and M. M. Micci. Development of a microwave resonant cavity electrothermal thruster prototype. In 23^{rd} *International Electric Propulsion Conference*, Seattle, WA, September 1993. IEPC-93-036.

[6] P. Balaam and M. M. Micci. Investigation of stabilized resonant cavity microwave plasmas for propulsion. *Journal of Propulsion and Power*, 11:1021–1027, 1995.

[7] D.A. Schwer, S. Venkateswaran, and C. L. Merkle. Analysis of microwave-heated rocket engines for space propulsion. In *AIAA* 29^{th} *Joint Propulsion Conference*, Monterey, CA, June 1993. AIAA 93-2105.

[8] R. Broglia, M. Manna, H. Deconinck, and G. Degrez. Development and validation of an axisymmetric navier-stokes solver for hypersonic flows. Technical Note 188, von Karman Institute for Fluid Dynamics, 1995.

[9] L. Martinelli. *Calculations of Viscous Flows with a Multigrid Method*. PhD thesis, Princeton University, 1987.

[10] G.L. Brown, A.P. Ratta, R.W. Anderson, L. Martinelli, W.R. Lempert, and R.B. Miles. Fluid mechanics in a radiatively driven hypseronic wind-tunnel - prediction and preliminary experiment. In 19^{rd} *AIAA Advanced Measurement and Ground Testing Technology Conference*, New Orleans, LA, June 1996. AIAA-96-2199.

[11] S. Gordon and B. J. McBride. Computer program for calculation of complex chemical equilibrium compositions and applications: Part 1 analysis. Reference Publication NASA-RP-1311, NASA Lewis Research Center, 1994.

[12] R.G. Jahn. *Physics of Electric Propulsion*. McGraw-Hill, 1968.